

Fast Computation of the Electrical Parameters of Sector-Shaped Cables using Single-Source Integral Equation and 2D Moment-Method Discretization

M. Shafieipour, J. De Silva, A. Kariyawasam, A. Menshov, V. Okhmatovski

Abstract— The per-unit-length capacitance of sector-shaped cables has been shown to remain relatively constant when operating in power system frequencies (up to 1MHz) making it possible to approximate it using closed-form expressions with reasonable accuracy. Numerical evaluation of frequency dependent resistance R and inductance L parameters of these types of cables remains computationally expensive. In this paper, the method-of-moment (MoM) discretization of the proximity- and skin-effect- aware formulation known as the surface-volume-surface electric field integral equation (SVS-EFIE) is optimized and applied for extracting the R and L parameters of circular and sector-shaped cables. While the proposed method guarantees to provide reliable data by iteratively achieving a desired accuracy, it also increases the efficiency of the MoM significantly. This makes the proposed method a suitable candidate for electromagnetic transient programs where rapid and accurate computation of the electrical parameters of sector-shaped cables is required.

Keywords: sector-shaped cables, electromagnetic transient program (EMTP), surface-volume-surface electric field integral equation (SVS-EFIE), method-of-moments (MoM).

I. INTRODUCTION

ELECTROMAGNETIC transient (EMT) analysis plays an important role in the design, operation, and performance of electrical power systems. As an important part of EMT, rapid and accurate computations of electrical per-unit-length (p.u.l.) parameters of various types of cables continues to be a sought-after subject. This is due to the fact that environmental, technical and political pressures dictate the use of various types of underground cables as opposed to the typical overhead lines. As an important example, sector-shaped cables are widely used at low and medium voltage levels in modern power systems. While the capacitance C parameter of sector-shaped cables remains almost unchanged from DC to 1MHz, the resistance R and inductance L of these types of cables varies significantly over such frequency range. Therefore, it is possible to accurately approximate C using closed-form expressions [1] but R and L should be computed using numerical techniques at different frequency points. In addition to the finite element method (FEM) [2] and conductor partitioning techniques [1], a new single-source integral equation formulation known as the

surface-volume-surface electric field integral equation (SVS-EFIE) discretized with the method-of-moments (MoM) is available for calculating R and L parameters of arbitrary shaped cables [3]. The SVS-EFIE is known to be a rigorous integral equation [4] and has been shown to accurately model proximity and skin effects [5]. While FEM, the sub-conductor technique, as well as the SVS-EFIE can accurately model sector-shaped cables, they often require substantial computational resources. This is primarily due to the large number of elements required to appropriately capture the pertinent fields especially at high frequencies where the size of the cable is large compared to the skin-depth. This makes efficient computations of the electrical parameters of sector-shaped cables a challenge in commercial EMT programs (EMTP).

In this paper, we optimize 2D MoM discretization of the SVS-EFIE by utilizing the following phenomena. 1) The skin-effect is used to reduce computations by knowing that the integral equation operators are negligible for surface elements that are far from the boundary. 2) A new adaptive meshing technique is proposed to ensure accurate results while saving CPU time and memory. 3) The matrix multiplication operations are done in order to gain memory efficiency at the expense of CPU time. 4) The process has been parallelized using shared-memory [6] parallel computing. 5) Comparison has been made on the performance of the C++ implementation when compiled with different compilers. These techniques combined, have allowed us to extract frequency dependent R and L parameters of sector-shaped cables with today's typical personal computer for 100 frequency points over several minutes, compared to several days required for the same example to complete using the non-optimized MoM solution. The accuracy of the proposed technique is validated by comparing results against commercial EMTP [7] and FEM [8] software.

II. THE PROPOSED OPTIMIZATION TECHNIQUES

Details of the SVS-EFIE formulation discretized with 2D MoM is given in [4] while references [3], [5] describe its usage in modeling cables of arbitrary shapes with single or multiple conductors. In this section, several optimization techniques are introduced for the work of [3]-[5] making it possible to

M. Shafieipour, J. De Silva, and A. Kariyawasam are with the Manitoba HVDC Research Centre, Canada (corresponding author email: mshafieipour@mhi.ca, email: jeewantha@psc.ad.com, akariyawasam@hvdc.ca).

A. Menshov is with the Department of Electrical and Computer Engineering, The University of Texas at Austin, United States (e-mail: anton.menshov@utexas.edu).

V. Okhmatovski is with the Department of Electrical and Computer

Engineering, University of Manitoba, Canada (e-mail: Vladimir.Okhmatovski@umanitoba.ca).

Paper submitted to the International Conference on Power Systems Transients (IPST2017) in Seoul, Republic of Korea June 26-29, 2017

efficiently compute R and L parameters using the SVS-EFIE.

A. Skin Effect

It is well established that an external electric field induces electromagnetic (EM) fields on the surface of a perfectly electric conducting (PEC) object and such fields do not penetrate into PECs [9]. On the other hand, for dielectric materials including non-perfect conductors such as copper and aluminum, the pertinent fields penetrate into the object but the fields' strength decay according to the frequency f and the object's material as $e^{-\delta}$ where $\delta = 1/\sqrt{\pi f \mu \sigma}$ is the skin-depth, μ is the permeability of the object, and σ is its conductivity. In an integral equation such as the SVS-EFIE, this indicates that the impact from the discretized integral operators contributing to the solution at an arbitrary observation point decrease in strength with $e^{-\delta}$ as the source point gets closer to the center of the conductor. Therefore, according to the desired accuracy, one can neglect elements of the mesh that are far from the boundary. For example, if 95% accuracy is required in the solution, the mesh elements further than $-\log(0.05)\delta=2.99\delta$ from the boundary have contributions less than 5% into *all* the integral operators and can be eliminated from *all* computations. Consequently, in computing the SVS-EFIE, one can consider elements of the mesh that are in the vicinity of the boundary up to 3δ only. This is demonstrated in Fig. 1.

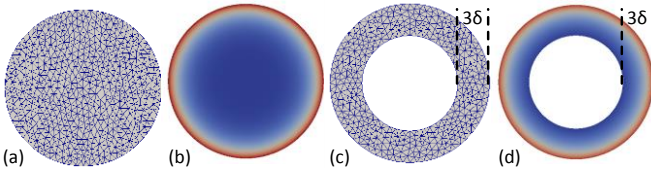


Fig. 1. In (a), the full cross-section of the conductor is meshed and (b) depicts the resulting surface current density computed by the SVS-EFIE. In (c), triangles beyond 3δ from the boundary are neglected and the resulting current density is depicted in (d). Both (a) and (c) share the same 1D mesh over the boundary of the real conductor. The p.u.l. impedance $Z=R+j\omega L$ computed from (d) match with Z computed from (b) with less than 5% deviation while the former (d) is computed using significantly less computational resources. Note that for hollow conductors the same principle applies which means that triangles close to both sides of the boundary need to be included in the mesh.

B. Adaptive Mesh Refinement

It is reasonable to suggest that for a computational EM (CEM) technique to produce acceptable results, at least 2 samples per wavelength is required for the discretization due to the Nyquist criterion (see [10, Sec. 5.2.1]). Therefore, in the classical volume electric field integral equation (V-EFIE) [11], typically 2 elements per skin-depth are used in the mesh. Due to the existence of two types of mesh elements (i.e. lines and triangles), in the MoM discretization of the SVS-EFIE [4], more research is required to formulate the optimal number of required 1D and/or 2D elements with respect to the skin-depth. This is because, the coefficients which are computed by SVS-EFIE correspond to the 1D lines over the boundary of the mesh ∂S , and not on the surface of the mesh S as in the classical V-EFIE. This is also different from classical surface integral equation techniques such as PMCHWT [9], where only the 1D elements of the boundary are considered. In this work, we follow the typical 2 samples per skin-depth over the cross-section but rely

on adaptive refinement of the 1D mesh until a desired accuracy is reached. To elaborate, by knowing that generally 2 triangles can fit into one quadrilateral of the same size (having circumscribing circle of the same radius) the largest triangle size in the mesh is set to 1δ to create the 2D mesh. This, by average, creates 2 samples per each direction of the 2D coordinate system. Then, a very coarse 1D mesh is created over the boundary. The area surrounded by this 1D mesh at the first iteration $S_{1D,iter1}$ is computed and stored. Without any EM computations, the 1D mesh is refined and $S_{1D,iter2}$ is computed. If the value of $|S_{1D,iter1} - S_{1D,iter2}| / |S_{1D,iter2}|$ is smaller than the acceptable tolerance (e.g. 0.05), either of the 1D meshes can be accepted for further computations, otherwise the refinement process is continued to have an accurate enough 1D mesh. This ensures that the 1D mesh can properly represent the true geometry and because there is no EM computations, such process is very fast. The above explained 1D and 2D meshes are used to obtain the p.u.l. impedance matrix $[Z]=[R]+j\omega[L]$ as explained in [3]-[5] and these values are stored in memory. In the next iteration, the 1D mesh is refined and the resulting cable parameters are compared against the parameters of the previous iteration. For the reasons that will be clear in Section III-A, the comparison is made for the magnitude of impedance parameters $|R+j\omega L|$, rather than R and L separately. This process is repeated until the compared results agree with no more than the acceptable tolerance in the solutions. As seen in Section III-B, this greatly improves the efficiency of the method while at the same time acts as a technique to numerically validate the final results. The increased efficiency is due to the reduction in the number of unknowns as a result of adaptively refining the mesh and is achieved despite the fact that the entire MoM procedure is repeated until the desired accuracy is reached.

C. Matrix Multiplications

The SVS-EFIE's MoM matrix $[Z_{MoM}]$ is written as [3]

$$[Z_{MoM}] = [Z_{\sigma}^{\partial S, \partial S}]_{M \times M} + [Z_0^{\partial S, S}]_{M \times N} \cdot [Z_{\sigma}^{S, \partial S}]_{N \times M} \quad (1)$$

$$= [Z_1] + [Z_2] \cdot [Z_3]$$

where M is the number of 1D (line) elements over the boundary of the mesh ∂S and N is the number of 2D (triangular) elements over the surface of the mesh S . Details of computing elements of (1) are found in [3]-[5]. The second line of (1) is given here to ease the subsequent discussion. The goal is to find the $(M \times 1)$ unknown coefficient matrix of the MoM $[I]$ as $([Z_1]+[Z_2] \cdot [Z_3]) \cdot [I]=[V]$ where $[V]$ is the $(M \times 1)$ matrix of the right-hand side. Hence it is possible to efficiently obtain matrix-vector product $([Z_1]+[Z_2] \cdot [Z_3]) \cdot [I]$ with iterative techniques such as the multilevel fast multipole algorithm [12]. However, in this work we limit ourselves to a direct inversion of $[Z_{MoM}]$ by LU-decomposition. This eliminates further complications that may arise due to iterative matrix implicit algorithms (e.g. conversion issues, need for preconditioners, additional error, etc.). It is important to realize that the size of $[Z_{MoM}]_{M \times M}$ is only related to the number of 1D elements over the boundary which is typically very small compared to the number of triangles over the surface (i.e. $M \ll N$). Utilizing the skin-effect as explained in Section II-A mitigates such difference by reducing the size

of $[Z_2]$ and $[Z_3]$, but they remain significantly larger than $[Z_{MoM}]$ especially at higher frequencies. For that reason, storing full matrices of $[Z_2]$ and $[Z_3]$ and computing their product, although efficient in terms of CPU time, is inefficient in terms of the memory requirement as it relates memory requirement to the number of triangles N . Therefore, the following procedure is proposed for computing and storing $[Z_{MoM}]$. First, the $(M \times M)$ matrix $[Z_1]$ is computed and stored into part of the memory where it is meant to hold the final matrix $[Z_{MoM}]$. Then, the first row of $[Z_2]$ and the first column of $[Z_3]$ are computed and used to update the element $[Z_{MoM}]_{1,1}$. By computing the second row of $[Z_2]$ and using the already available first row of $[Z_3]$, the element $[Z_{MoM}]_{2,1}$ is updated. This procedure is continued, until all elements of $[Z_{MoM}]$ are updated to form the final $[Z_{MoM}]$ as depicted in Fig. 2. As shown in the figure, such a way of computing and saving the final matrix $[Z_{MoM}]$, requires saving of an $(M \times M)$ matrix and a vector of size N , hence keeping the memory requirement to a minimum. However, this requires re-computing the matrix $[Z_2]$, M times, as for every column of $[Z_3]$ all elements of $[Z_2]$ are needed. Such re-computations do not have severe impact on the performance and are preferred over the saving of $[Z_2]$ for the following reasons; computing entries of $[Z_2]$ only require cheap evaluation of the logarithmic kernel [4], size of $[Z_2]$ decreases by reducing the surface mesh (Section II-A), and independent computation of $[Z_2]$ is suitable for parallelization as explained in the sequel.

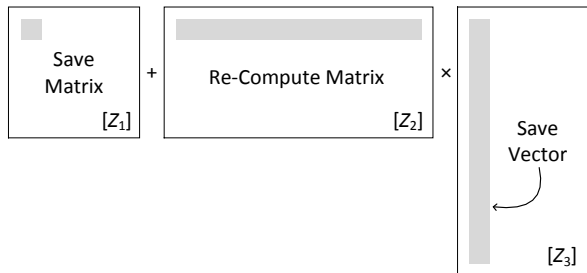


Fig. 2. Efficient computation and saving of $[Z_{MoM}]$ in (1).

D. Parallelization

There has been a growing interest towards parallel computing, especially in the past decade due to the abundant availability of parallel computing hardware [6]. Nowadays, in addition to readily available distributed memory servers, commodity personal computers are equipped with multi-core CPUs. Therefore, it is important to investigate parallelization when a new algorithm is introduced. In [12], it was shown that an integral equation technique of CEM can efficiently be parallelized for distributed memory systems. Similarly, the MoM solution of the SVS-EFIE can be parallelized for such systems to achieve satisfactory speed-ups (this will be a subject of future work). In this work, we parallelize the algorithm for shared-memory parallel computers for two reasons: 1) the majority of EMTP users run the software on workstations, and 2) converting a serial code to a shared-memory parallel code can be achieved using available libraries such as OpenMP [13] with minimal effort (i.e. by simply using OpenMP's `#pragma` directives before the existing loops and ensuring data locale). As demonstrated in Section III-B, the MoM discretization of the SVS-EFIE achieves satisfactory speed-ups when running over

a typical 4 core hyper-threaded CPU (8 threads). This is achieved in-part due to the matrix multiplication technique explained in the previous section. Re-computing the matrix of $[Z_2]$ for every column of $[Z_3]$, is parallelized with optimal parallel efficiency due to the possibility of independently computing $[Z_2]$ on different cores. Therefore, such matrix multiplication and parallelization, can be seen as exchanging CPU power for memory. This is desirable as usually in integral equation techniques of CEM memory constraints are the limiting factor rather than CPU constraints. It is worth noting that SVS-EFIE is special among available integral equations. Volume integral equations such as V-EFIE suffer from too many unknowns. Surface integral equations such as PMCHWT and EFIE/MFIE for dielectrics [9] are not single-source and require at least twice the number of unknowns compared to SVS-EFIE, assuming that the discretizations are done in a similar manner. Alternative single-source integral equations [14] feature large number of integral operator products and are more difficult to solve especially when planar layered media is to be included [15]. This makes the impedance matrix of the SVS-EFIE one of the most efficient amongst the available integral equation techniques. The downside of the SVS-EFIE is the memory requirement for computing $[Z_2] \cdot [Z_3]$, but as was explained earlier, it can be overcome by exchanging CPU power for memory. Moreover, graphics processing units which have been shown to accelerate EMT simulations [16], may be able to help further speed-up computation of $[Z_2] \cdot [Z_3]$. Such study is left for future publications.

E. C++ Compiler

When an algorithm is implemented in a programming language, one needs to choose a suitable compiler for that particular algorithm and implementation. Many factors may contribute to such choice. For example, the operating system, the budget, the licensing, etc. Two compilers were considered in this work, the Visual C++ Compiler which is included in Microsoft's Visual Studio [17], and the Intel C++ Compiler [18]. The code was compiled using both compilers with a similar set of compilation flags. The two executables were run for the same examples. As exemplified in Section III-B, in almost all cases, the executable that was compiled using the Intel C++ compiler, was more than twice as fast in providing identical results. Reasons are beyond the scope of this paper and are subject to future studies. Note that the compilation time itself is negligible for both compilers and thus not included in the study. In this work, the Intel MKL [19] with no additional template library [20] was used for inverting $[Z_{MoM}]$.

III. RESULTS AND DISCUSSION

A. Study of Accuracy

In order to comprehensively validate the accuracy of the proposed method, we apply all the optimization techniques of Section II to SVS-EFIE and compare the results with that of commercial EMTP (PSCAD [7]) and FEM (COMSOL [8]) software. For comparison, the relative error is used as

$$Err(X_{test}) = |X_{test} - X_{ref}| / |X_{ref}| \quad (2)$$

where X_{test} is the numerical value under test and X_{ref} is the numerical value taken as the reference solution. In all simulations herein, the skin-effect (Section II-A) and the adaptive mesh refinement (Section II-B) are requested to be accurate with no more than 5% relative error. This means that only triangular elements that are 3δ in the vicinity of the boundary are considered (e.g. Fig. 1c) and the impedance is iteratively computed until less than 5% relative error is seen between the last two solutions.

In the context of EMTP, an earth return representation is required to properly model underground cables. This is typically done using analytical approximations or direct numerical integration [7]. In this paper, we use an analytical formula (i.e. (6) of [21]) to approximate the earth return impedance Z_0 . Therefore, FEM and SVS-EFIE are computed in free-space and each entry of the resulting impedance matrix $[Z]$ is added to Z_0 to produce results that can be compared with that of EMTP. To have large enough free-space around the conductor in FEM, the ground surface is established at 1m from the geometrical center of the cross-section (set at origin) and for consistency, the SVS-EFIE is also referenced at 1m. This means that in COMSOL the air surrounding the cable has circular cross-section bounded with conductor boundary of 1m radius. In SVS-EFIE, the Green's function is set to zero at 1m away from the origin [4]. The discrepancy between the actual radius of the outermost surface of the cable and the considered 1m radius is compensated by computing Z_0 for a cable with outermost radius of 1m as well.

First, comparison is made for the cable shown in Fig. 1 where the radius of the conductor (copper) is 22mm, the insulator surrounding the copper has radius of 39.5mm, and the cable is situated 2m below ground where the resistivity of the soil is uniform and equal to $100\Omega\cdot\text{m}$. Note that unlike the capacitance, the resistance and inductance parameters are independent of the permittivity ϵ of insulators and thus ϵ is not important in our study. Fig. 3 presents the relative error (2) in R and L values where EMTP is used as the reference solution. The maximum relative error in Fig. 3 is 4.77%. This demonstrates that despite all the optimization techniques introduced in this paper, the SVS-EFIE produces reliable results for a cable with circular cross-section. This also indicates that our setup for FEM properly match with that of EMTP. Similar observations are made in the presence of multiple coaxial cables with and without single or multiple sheath layers.

Next, we compare results of the proposed technique with that of FEM for the sector-shaped cable shown in Fig. 4. For this example, EMTP results are not available. Again, both FEM and SVS-EFIE are solved in air and terminated at 1m while Z_0 is analytically computed for the same 1m radius. Due to symmetry, the impedance matrix has the following form

$$[Z] = \begin{bmatrix} Z_1 & Z_2 & Z_3 & Z_2 & Z_4 \\ Z_2 & Z_1 & Z_2 & Z_3 & Z_4 \\ Z_3 & Z_2 & Z_1 & Z_2 & Z_4 \\ Z_2 & Z_3 & Z_2 & Z_1 & Z_4 \\ Z_4 & Z_4 & Z_4 & Z_4 & Z_5 \end{bmatrix} \quad (3)$$

where Z_1 is the self-impedance of each sector, Z_2 is the mutual impedance of two adjacent sectors, Z_3 is the mutual impedance

of two non-adjacent sectors, Z_4 is the mutual impedance of each sector and the sheath, and Z_5 is the self-impedance of the sheath. TABLE I presents the results where numbers are rounded to three significant digits. FEM and SVS-EFIE are numerical techniques that solve for the current density J (rather than R and L) over the 2D cross-section of Fig. 4. By exciting one conductor at a time with -1V p.u.l. and summing J over each conductor for every excitation, a (5×5) admittance matrix $[Y]$ is obtained. By inverting $[Y]$, the impedance matrix $[Z]$ of (3) is then computed where real values represent R and imaginary values represent ωL . This has a very important numerical consequence. The impedance values are accurate with 2 to 3 digits of precision for their magnitude ($|Z_i|$ in the table) and not real and imaginary parts separately. For example, by comparing the values of Z_3 at 1Hz computed by the two techniques in TABLE I, it is realized that while the imaginary parts representing the inductance values ωL match ($4.60E-06i$), the real values representing the resistance are negative (non-physical) and do not match with each other. This is because the imaginary part of Z_3 is about 3 orders of magnitude larger than its real part and hence the real part lies below the noise floor of the used numerical techniques. Such numerical inaccuracy cannot efficiently be reduced unless FEM or SVS-EFIE are discretized using high-order techniques (see [10, Sec. 5.4] and [22]). For example, it was not possible for us to obtain non-negative resistive values with FEM by progressively refining

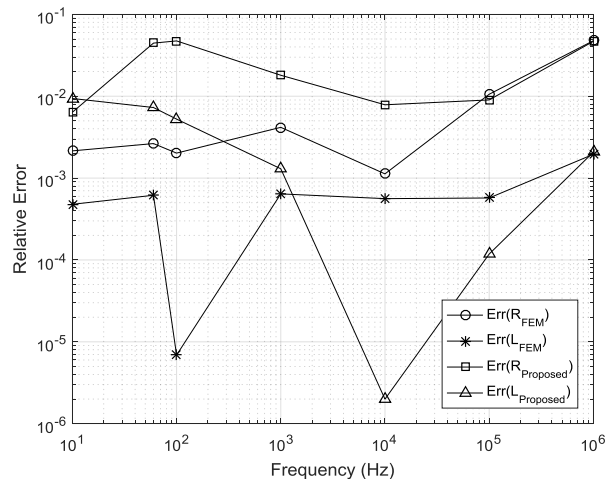


Fig. 3. The relative error in the proposed technique and FEM for the example shown in Fig. 1 where radius is 22mm. To compute the relative error, R_{EMTP} and L_{EMTP} [7] are used as the reference solution in (2).

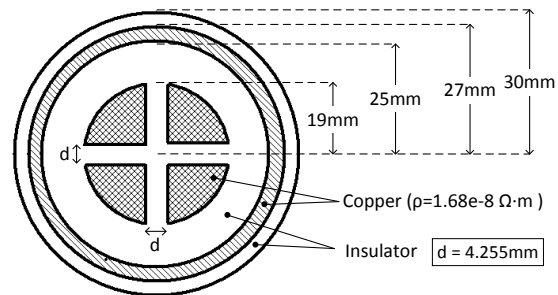


Fig. 4. The sector-shaped cable under study. Resistivity of copper is $1.68e-8 \Omega\cdot\text{m}$ and the center of the cable is assumed to be 2 meters below ground with uniform resistivity of $100 \Omega\cdot\text{m}$. The relative permeability is $\mu_r=1$ everywhere. The relative permittivity of insulators does not contribute to R and L parameters.

TABLE I
THE IMPEDANCE VALUES OF (3) FOR THE SECTOR-SHAPED CABLE OF FIG. 4 COMPUTED IN FREE-SPACE

Method	Z_1	Z_2	Z_3	Z_4	Z_5
FEM, 1Hz	8.08E-05+6.31E-06i	7.20E-10+5.04E-06i	-3.95E-09+4.60E-06i	7.37E-12+4.59E-06i	5.14E-05+4.59E-06i
Proposed, 1Hz	8.21E-05+6.19E-06i	-8.97E-10+5.04E-06i	-5.22E-09+4.60E-06i	-3.25E-12+4.59E-06i	5.16E-05+4.62E-06i
FEM, 10Hz	8.15E-05+6.30E-05i	6.51E-08+5.04E-05i	-3.88E-07+4.60E-05i	-1.27E-09+4.59E-05i	5.14E-05+4.59E-05i
Proposed, 10Hz	8.20E-05+6.31E-05i	6.28E-08+5.04E-05i	-3.87E-07+4.60E-05i	3.98E-10+4.59E-05i	5.14E-05+4.57E-05i
FEM, 60Hz	9.69E-05+3.68E-04i	2.10E-06+3.02E-04i	-7.04E-06+2.83E-04i	5.35E-09+2.75E-04i	5.14E-05+2.75E-04i
Proposed, 60Hz	9.71E-05+3.68E-04i	2.09E-06+3.01E-04i	-7.04E-06+2.83E-04i	2.22E-08+2.75E-04i	5.14E-05+2.74E-04i
FEM, 100Hz	1.11E-04+6.01E-04i	4.79E-06+5.01E-04i	-9.06E-06+4.78E-04i	3.67E-08+4.59E-04i	5.14E-05+4.59E-04i
Proposed, 100Hz	1.11E-04+6.01E-04i	4.78E-06+5.01E-04i	-9.07E-06+4.78E-04i	6.64E-08+4.59E-04i	5.15E-05+4.57E-04i
FEM, 1kHz	2.82E-04+5.58E-03i	4.29E-05+4.93E-03i	8.41E-06+4.80E-03i	7.03E-06+4.58E-03i	5.50E-05+4.58E-03i
Proposed, 1kHz	2.40E-04+5.52E-03i	4.10E-05+4.92E-03i	6.68E-06+4.80E-03i	6.25E-06+4.59E-03i	5.44E-05+4.57E-03i
FEM, 10kHz	1.39E-03+5.34E-02i	5.46E-04+4.84E-02i	4.03E-04+4.74E-02i	2.13E-04+4.55E-02i	1.79E-04+4.55E-02i
Proposed, 10kHz	9.91E-04+5.34E-02i	4.61E-04+4.85E-02i	3.64E-04+4.74E-02i	1.89E-04+4.56E-02i	1.50E-04+4.55E-02i
FEM, 100kHz	2.45E-03+5.24E-01i	8.74E-04+4.80E-01i	5.91E-04+4.71E-01i	3.06E-04+4.54E-01i	4.29E-04+4.54E-01i
Proposed, 100kHz	2.76E-03+5.28E-01i	1.11E-03+4.81E-01i	8.17E-04+4.71E-01i	4.20E-04+4.54E-01i	3.89E-04+4.54E-01i
FEM, 1MHz	2.50E-03+5.24E+00i	8.93E-04+4.80E+00i	6.01E-04+4.71E+00i	3.12E-04+4.54E+00i	4.55E-04+4.54E+00i
Proposed, 1MHz	8.46E-03+5.26E+00i	3.23E-03+4.81E+00i	2.32E-03+4.71E+00i	1.20E-03+4.54E+00i	1.17E-03+4.54E+00i

the mesh. For SVS-EFIE, we eliminated all the introduced optimization techniques and used more than 2 samples per δ in the hope that such numerical error disappear to no avail. In fact, as long as a numerical technique solves for the current density J (rather than separately for R and L) and is discretized using low-order methods, it will not produce reliable R parameters where ωL is much larger than R . This may occur throughout the studied frequency range (see also Z_5 at 1MHz). Nevertheless, EMTP requires adding Z_0 to the impedance values computed by FEM and SVS-EFIE as was done in Fig. 3 where results of FEM and the proposed technique were matched with that of EMTP. Such addition circumvents the above explained numerical issue as the real part of Z_0 dominates the final resistive value where the real part of Z_i is small compared to its imaginary part. Fig. 5 plots the FEM and SVS-EFIE resistance values obtained from Z_i+Z_0 where Z_i is taken from TABLE I and Z_0 is analytically computed [21] for depth of 2m (TABLE II). It can be seen that the resistance values of FEM and SVS-EFIE match while their behavior is consistent with the physical characteristics of the cable (e.g. positive values, larger self-resistances compared to mutual-resistances at lower frequencies, etc). By extracting the parameters from Z_i+Z_0 , the largest deviation (2) between results of FEM and the proposed technique in R and L are 3.4% (Fig. 5) and 0.8%, respectively. This is consistent with the 5% error tolerance set for the optimized SVS-EFIE. Similar observations are made if Z_0 is computed for different depths. Therefore, despite the accuracy in $|Z|$ rather than separately for R and L , the proposed technique can provide reliable R and L parameters which can effectively be used in EMTP.

B. Study of Efficiency

In this section we run the SVS-EFIE for the example shown in Fig. 4 with and without the optimization techniques over 100 frequencies ($0.5\text{Hz} \leq f \leq 1\text{MHz}$). The studies are done on a machine with Intel Core i7-3920XM CPU with 3.1 GHz max frequency. It has 4 physical cores with 8 threads and 16GB of

memory. Results are shown in TABLE III. It can be seen that the efficient matrix multiplication procedure explained in Section II-C is essential to running such example. Without it, the 16GB machine would not have sufficient memory to run the example at higher frequencies. By using the Intel C++ Compiler, a speed-up of 2.45 times has been gained where over the frequency range, the speed-up varies from about $\times 2.2$ to $\times 2.6$ with almost linear increase from lower to higher frequencies. From TABLE III, it can be seen that the parallel efficiency is about 54% over 8 threads. This is acceptable

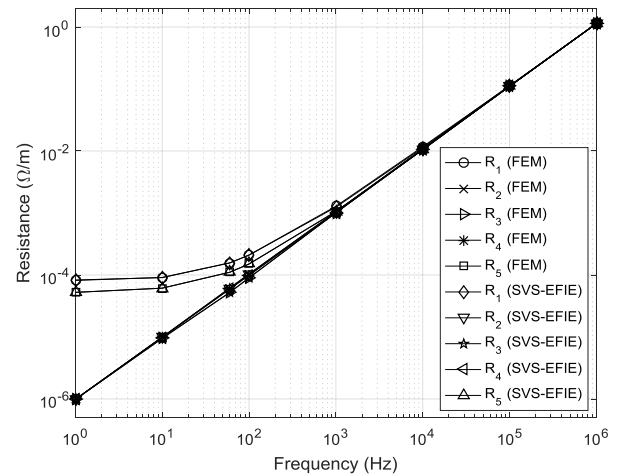


Fig. 5. The resistance $R_i = \text{real}(Z_i + Z_0)$ of the sector shaped cable shown in Fig. 4 where Z_i is computed by FEM and SVS-EFIE (TABLE I) and Z_0 is analytically computed (TABLE II). The maximum relative error (2) is 3.4%.

TABLE II
THE EARTH RETURN IMPEDANCE FOR 1M RADIUS CABLE 2M BELOW GROUND

Freq.	1Hz	10Hz	60Hz	100Hz
Z_0	9.87E-07+ 1.10E-05i	9.89E-06+ 9.60E-05i	5.94E-05+ 5.08E-04i	9.92E-05+ 8.15E-04i
Freq.	1kHz	10kHz	100kHz	1MHz
Z_0	1.00E-03+ 6.69E-03i	1.03E-02+ 5.21E-02i	1.10E-01+ 3.66E-01i	1.13E+00+ 1.95E+00i

speed-up considering that the machine has 4 physical cores and hyper-threading has resulted in 8 OpenMP threads. This table also demonstrates the significant speed-ups of over 13 and 7 times by using the skin-effect and adaptive meshing technique, respectively. Fig. 6 compares the meshes which were used in TABLE III at 1MHz. It demonstrates the advantages of adopting the proposed techniques in creating an efficient mesh for the 2D MoM discretization of the SVS-EFIE to not only speed-up the process but also guarantee reliable results by running MoM iteratively until the desired accuracy is achieved.

TABLE III

RUNTIME DETAIL FOR THE STUDY OF THE EFFICIENCY FOR 100 FREQUENCIES

Technique	Time taken	Speed-up w.r.t. previous	Speed-up w.r.t. A+B
A	The 16GB machine runs out of memory		
A+B	8d:1h:9m:20s	-	×1
A+B+C	3d:6h:48m:25s	×2.45	×2.45
A+B+C+D	18h:3m:9s	×4.36	×10.7
A+B+C+D+E	1h:21m:21s	×13.31	×142.46
A+B+C+D+E+F	11m:29s	×7.08	×1009.23

A = SVS-EFIE ([3]-[5]), B = Efficient matrix multiplication (Section II-C), C = Intel C++ Compiler (Section II-E), D = Shared-memory parallelization (Section II-D), E = Utilizing Skin-Effect (Section II-A), F = Adaptive mesh refinement (Section II-B)

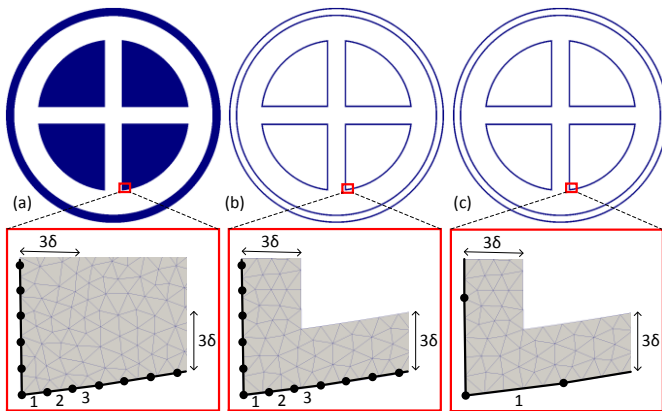


Fig. 6. Comparison of the three meshes used in TABLE III at 1MHz. The full mesh (a) was used in A, A+B, A+B+C, and A+B+C+D in which for every 4 triangles at the boundary, 3 line elements were considered. By making the size of each triangle to 1 δ , the Nyquist 2 samples per each direction of the 2D surface is achieved. This resulted in 362,548 triangles and 5,344 line elements. By neglecting triangles further than 3 δ from all boundaries (b), the number of triangles has been reduced to 42,656 in A+B+C+D+E while the same number of 1D elements (5,344) are used. Finally in (c), in addition to considering 42,656 2D elements, the adaptive meshing technique has reduced the number of line elements (also unknowns) to 1,230 which was used in A+B+C+D+E+F.

IV. CONCLUSIONS

This paper introduces optimization techniques for obtaining the R and L parameters of cables using the SVS-EFIE. These methods not only guarantee to provide reliable results, they also increase the efficiency, significantly. For example, over 100 frequency points, the runtime has been reduced from over 8 days to under 12 minutes for a realistic sector-shaped cable model. While these techniques can be used for any arbitrary shaped cable, the fact that the capacitance should be approximated by analytical formulas, the discussion of this paper is limited to circular and sector-shaped cables. In fact, this work along with closed-form approximation of C for sector-

shaped cables is currently being considered for inclusion in the commercial software PSCAD. In future work, we introduce a technique to numerically evaluate C for arbitrary shaped cables making it possible to efficiently compute electrical parameters of cables with arbitrary cross-sections in EMTP.

V. REFERENCES

- [1] K.K.M.A. Kariyawasam, A. M. Gole, B. Kordi, H.M.J.S.P. De Silva, "Accurate Electromagnetic Transient Modelling of Sector-Shaped Cables", in *IPST*, Delft, The Netherlands, June 2011.
- [2] B. Gustavsen, A. Bruaset, J. J. Bremnes and A. Hassel, "A Finite-Element Approach for Calculating Electrical Parameters of Umbilical Cables," *IEEE Trans. Power Delivery*, vol. 24, no. 4, pp. 2375-2384, Oct. 2009.
- [3] A. Menshov, V. Okhmatovski, H.M.J.S.P. De Silva, K.K.M.A. Kariyawasam, J. E. Nordstrom, "Modeling of Arbitrary Shaped Cables Using Novel Single Source Integral Equation Formulation", in *IPST*, Catvat, Croatia, June 2015.
- [4] A. Menshov and V. Okhmatovski, "New Single-Source Surface Integral Equations for Scattering on Penetrable Cylinders and Current Flow Modeling in 2-D Conductors," *IEEE Trans. Microw. Theory Tech.*, vol. 61, no. 1, pp. 341-350, Jan. 2013.
- [5] A. Menshov and V. Okhmatovski, "Novel Surface Integral Equation Formulation for Accurate Broadband RL Extraction in Transmission Lines of Arbitrary Cross-Section," in *IMS*, Montreal, Canada, Jun. 2012.
- [6] B. Wilkinson and M. Allen, *Parallel Programming: Techniques and Applications Using Networked Workstations and Parallel Computers*, Pearson; 2nd ed., March 2004.
- [7] Manitoba Hydro International Ltd. (Jan. 18, 2017). *PSCAD/EMTDC*. [Online]. Available: <https://hvdc.ca/pscad>
- [8] COMSOL Inc. (Jan. 18, 2017). *COMSOL Multiphysics*. [Online]. Available: <https://www.comsol.com/comsol-multiphysics>
- [9] A. Peterson, S. Ray, and R. Mittra, *Computational Methods for Electromagnetics*, Piscataway, NJ; IEEE Press, 1998.
- [10] M. Shafieipour, "Efficient Error-Controllable High-Order Electromagnetic Modelling of Scattering on Electrically Large Targets with the Locally Corrected Nyström Method," Ph.D. dissertation, Dept. Elect. Comput. Eng., Univ. Manitoba, Winnipeg, MB, Canada, 2016. [Online]. Available: <http://hdl.handle.net/1993/31181>
- [11] W. C. Chew, *Waves and Field in Inhomogeneous Media*, Piscataway, NJ; IEEE Press, 1995.
- [12] I. Jeffrey, J. Aronsson, M. Shafieipour, and V. Okhmatovski, "Error Controllable Solutions of Large Scale Problems in Electromagnetics: MLFMA Accelerated Locally Corrected Nyström Solutions of CFIE in 3D," *IEEE Antennas Propag. Mag.*, vol. 55, no. 3, pp. 294-308, Jun. 2013.
- [13] OpenMP (Jan. 19, 2017). [Online]. Available: <http://www.openmp.org/>
- [14] U. R. Patel and P. Triverio, "Skin Effect Modeling in Conductors of Arbitrary Shape Through a Surface Admittance Operator and the Contour Integral Method," *IEEE Trans. Microw. Theory Tech.*, vol. 64, no. 9, pp. 2708-2717, Sep. 2016.
- [15] S. Zheng, A. Menshov and V. I. Okhmatovski, "New Single-Source Surface Integral Equation for Magneto-Quasi-Static Characterization of Transmission Lines Situated in Multilayered Media," *IEEE Trans. Microw. Theory Tech.*, vol. 64, no. 12, pp. 4341-4351, Dec. 2016.
- [16] J. K. Debnath, A. M. Gole and W. K. Fung, "Graphics-Processing-Unit-Based Acceleration of Electromagnetic Transients Simulation," *IEEE Trans. Power Delivery*, vol. 31, no. 5, pp. 2036-2044, Oct. 2016.
- [17] Microsoft Corporation (Jan. 19, 2017). *Visual Studio 2010*. [Online]. Available: <https://www.visualstudio.com/>
- [18] Intel Corporation (Jan. 19, 2017). *Intel C++ Compilers*. [Online]. Available: <https://software.intel.com/en-us/c-compilers>
- [19] Intel Corporation (Jan. 19, 2017). *Intel Math Kernel Library (Intel MKL)*. [Online]. Available: <https://software.intel.com/en-us/intel-mkl>
- [20] Eigen+MKL vs. MKL-Only (Jan. 19, 2017). [Online]. Available: <https://software.intel.com/en-us/forums/intel-math-kernel-library/topic/670435>
- [21] O. Saad, G. Gaba and M. Giroux, "A Closed-Form Approximation for Ground Return Impedance of Underground Cables," *IEEE Trans. Power Delivery*, vol. 11, no. 3, pp. 1536-1545, Jul. 1996.
- [22] F. Sheikh Hosseini Lori, M. S. Hosen, A. Menshov, M. Shafieipour, and V. Okhmatovski, "Accurate Transmission Lines Characterization via Higher Order Moment Method Solution of Novel Single-Source Integral Equation", in *IEEE MTT-S Int. Microw. Symp. Dig.*, Jun. 4-9, 2017, pp. 1-3, accepted.